Applied Clay Science 135 (2017) 282–288

Contents lists available at ScienceDirect

Applied Clay Science

journal homepage: www.elsevier.com/locate/clay

Research paper

Metal occupancy and its influence on thermal stability of synthetic saponites

Chaoqun Zhang [a,b,c], Hongping He [a,b], Qi Tao [a,b], Shichao Ji [a,b,c], Shangying Li [a,b,c], Lingya Ma [a,b], Xiaoli Su [a,b,c], Jianxi Zhu [a,b,*]

[a] Key Laboratory of Mineralogy and Metallogeny, Guangzhou Institute of Geochemistry, Chinese Academy of Sciences, Guangzhou 510640, China
[b] Guangdong Provincial Key Laboratory of Mineral Physics and Materials, Guangzhou 510640, China
[c] University of Chinese Academy of Sciences, Beijing 100049, China

ARTICLE INFO

Article history:
Received 15 August 2016
Received in revised form 2 October 2016
Accepted 4 October 2016
Available online 19 October 2016

Keywords:
Synthetic saponite
Metal occupancy
Thermal stability
Isomorphous substitution

ABSTRACT

Due to high surface acidity and thermal stability, saponite has important applications in various fields. In this study, saponites with different Mg/Zn ratios (0–6) and a fixed Si/Al ratio of 5.43 were synthesized under hydrothermal condition. The resultant synthetic saponites were characterized by using XRD, FTIR, TG, SEM and MAS NMR. The characterization results demonstrated that, with a decrease of Mg/Zn ratio, both the crystallinity and layer stacking order of saponite were increased, and rose-like morphology was observed in Zn-saponite. Al^{3+} preferentially occupied tetrahedral sites in *Si*-O tetrahedral sheet in all synthetic saponites. A decrease of Mg/Zn ratio in octahedral sheet could improve the substitution extent of Al^{3+} for Si^{4+} and resulted in an increase of Al(IV)/Al(VI) ratio in the resultant saponite, which might be a crucial factor to control the crystal growth of saponite. The dehydroxylation temperature of saponite depended strongly on the Mg/Zn ratio and the replacement of Al^{3+} for Mg^{2+} and Zn^{2+} in octahedral sheets, due to their different bond strength. A 'one-to-one' mode was proposed for the substitution of Al^{3+} for Mg^{2+} and Zn^{2+} in octahedral sheets of the synthetic saponites.

1. Introduction

Saponite is a kind of 2:1 type trioctahedral phyllosilicate, belonging to smectite group clay minerals. In its unit layer, a central $MgO_4(OH)_2$ octahedral sheet is sandwiched by two *Si*-O tetrahedral sheets via sharing oxygen. The ideal structural formula of saponite can be expressed as $M+X\,[Si_{4-x}Al_x][Mg_3]O_{10}(OH)_2\cdot nH_2O$, where *M* is the exchangeable interlayer cation, *x* ($0.2 \le x \le 1.2$) is the fraction of aluminum present in *Si*-O tetrahedral sheet, and *n* is the number of water molecules (Kloprogge et al., 1994; Vogels et al., 2005a; Costenaro et al., 2013). As shown by saponite formula, negative charges for saponite layers are created mainly by the isomorphous substitution of Al^{3+} for Si^{4+} in the tetrahedral sheet, which are compensated by exchangeable interlayer cations such as Na^+, Ca^{2+}, and Mg^{2+}. The octahedral sites are generally occupied by Mg^{2+} in nature, and can be substituted by other cations such as Al^{3+}, Fe^{3+}, Li^+, Mn^{2+}, Ni^{2+}, and Zn^{2+} (Mackenzie, 1957; Rodriguez et al., 1994; Varma, 2002).

Due to the high surface acidity and thermal stability, saponite has many important applications in a number of fields, including clay-based polymer nanocomposites and heterogeneous catalysts (Varma, 2002; Casagrande et al., 2005; Liu and Breen, 2005). However, the chemical composition and physicochemical properties of natural saponites are extremely variable, which depend on the chemical compositions of the mother rocks, the genesis process and the provenance (Utracki, 2007). Thus, natural saponite cannot meet the requirements in some fields such as catalysts, in which the chemical composition and surface property are required to be homogeneous (Artok et al., 1993; Chevalier et al., 1994). The composition and property variability of natural saponites strongly limits their industrial applications. For this reason, different methods have been developed to synthesize saponites with well-controlled chemical composition and property (Farmer et al., 1991; Kloprogge et al., 1993; Vogels et al., 1997; Kawi and Yao, 1999; Jaber et al., 2005; Higashi et al., 2007; Bisio et al., 2008; Vicente et al., 2010). More importantly, saponite-type clay minerals can be obtained by synthesis ways, which are rare in nature but have unique property and morphology (Zhang et al., 2010).

Saponites with various metals in octahedral sheet (i.e., Mg^{2+}, Zn^{2+}, Ni^{2+}, Cu^{2+}, Co^{2+}) have been successfully synthesized, and their structure and properties (e.g., specific surface area, lateral size, order of layer stacking) were investigated (Brtndle and KrrKewe, 1979; Brat and Rajan, 1981; Decarreau et al., 1992; Grauby et al., 1994; Reinholdt et al., 2005; Trujillano et al., 2015). Vogels et al. (2005b) proposed that

* Corresponding author at: Guangzhou Institute of Geochemistry, Chinese Academy of Sciences, No. 511 Kehua Street, Tianhe District, Guangzhou 510640, China.
E-mail address: zhujx@gig.ac.cn (J. Zhu).

http://dx.doi.org/10.1016/j.clay.2016.10.006
0169-1317/

the compositions of the octahedral and tetrahedral sheets had significant influences on the structure and physicochemical property of synthetic saponites. For example, the crystal size of Mg-saponite is smaller than that of Zn-saponite, and the average stacking degree of the saponite layers is higher in Zn-saponite than that in Mg-saponite. Correspondingly, Mg-saponite has higher micropore volume and specific surface area than Zn-saponite (Vogels et al., 1995; Vogels et al., 2005b). Meanwhile, Mg-saponite had higher Brönsted acid density than Zn-saponite (Leliveld et al., 1998). However, saponite containing both Zn^{2+} and Mg^{2+} in octahedral sheets displayed better catalytic activity in alcohol decomposition and cumene cracking (Prikhod'ko et al., 2003). These differences on the structure and property of synthetic saponite may be controlled by the occupancy of Al^{3+} in saponite, besides the effects of the nature of Mg^{2+} and Zn^{2+} and their distribution. The substitution of Al^{3+} for Si^{4+} is critical for growth of saponite crystals (He et al., 2014) and can produce Brönsted acid sites (Suquet et al. 1981). Prikhod'ko et al. (2003) suggested that the preferential occupancy of Al^{3+} in the tetrahedral sheet of Mg- and Zn-saponite only occurred when the atomic ratio $Si^{4+}/Al^{3+} \geq 12$ (Prikhod'ko et al., 2003). However, He et al. (2014) demonstrated that Al^{3+} preferred to occupy tetrahedral sites instead of octahedral ones in Mg-saponite with different Si/Al ratios. Moreover, both the saponite crystallinity and the layer stacking order are controlled by the distribution fraction of Al^{3+} in tetrahedral and octahedral sheets (i.e., the ratio of Al(IV)/Al(VI)). It is noteworthy that, in a ternary system of octahedral sheet (i.e., Mg-Zn-Al), the ratio of Mg/Zn may have a significant effect on the distribution of Al^{3+} in tetrahedral and octahedral sheets and a further influence on the structure and property of the resultant saponite, which has not been systematically investigated.

Hence, the main aim of this study is to investigate metal distribution and its influence on thermal stability of synthetic saponites with different Mg/Zn ratios. The saponites were synthesized under hydrothermal condition and characterized by using a combination of techniques, including X-ray diffraction (XRD), Fourier-transform infrared spectroscopy (FTIR), thermogravimetric analysis (TG), scanning electron microscopy (SEM), and ^{27}Al and ^{29}Si solid-state magic-angle-spinning nuclear magnetic resonance spectroscopy (MAS NMR). The insights about the effect of Mg/Zn ratio on the occupancy of Al^{3+} in tetrahedral and octahedral sheets and the thermal stability of synthetic saponites are of high importance for synthesis and application of synthetic saponite.

2. Experimental

2.1. Sample preparation

Saponite samples with a fixed ratio Si/Al/(Mg + Zn) of 1.18, and Mg/Zn ratios of 6, 4, 2, and 0, respectively, were prepared by modifying a previously reported method (Kawi and Yao 1999).

A general synthesis procedure is as follows: A mixture of 4.00 g of NaOH and 9.00 g of $NaHCO_3$ was dissolved in 125 mL deionized water. Then, 24.00 g of sodium metasilicate ($Na_2SiO_3 \cdot 9H_2O$) solution was added to the buffer solution under vigorous stirring (Solution A). Desired amounts of $MgCl_2 \cdot 6H_2O$, $ZnCl_2$ and 3.80 g of $AlCl_3 \cdot 6H_2O$ were dissolved in 12.5 mL of deionized water (Solution B). With continuous stirring, Solution B was slowly added into Solution A until a uniform gel was eventually formed. The gel was then transferred to a polytetrafluoroethylene-lined autoclave and heated at 200 °C for 72 h. The obtained products were denoted as Sap-Mg6Zn0, Sap-Mg4Zn2, Sap-Mg2Zn4, and Sap-Mg0Zn6, respectively.

2.2. Characterization

2.2.1. X-ray diffraction (XRD)

Randomly oriented powder XRD patterns were collected from 3° to 80° (2θ) at a scanning rate of 1° (2θ) min^{-1} on a Bruker D8 Advance diffractometer with Ni-filtered CuKα radiation (λ = 0.154 nm, 40 kV, and 40 mA).

2.2.2. Thermogravimetric analysis (TG)

TG analysis was conducted on a Netzsch STA 409PC instrument. Approximately 10 mg of the sample was heated in a corundum crucible. The sample was heated from 30 to 1000 °C at a heating rate of 10 °C/min under a highly pure N_2 atmosphere (60 cm^3/min).

2.2.3. Fourier-transform infrared spectroscopy (FTIR)

FTIR spectra of the samples were recorded on a Bruker Vertex-70 Fourier-transform infrared spectrometer. The specimens were prepared for measurement by mixing 0.9 mg of the sample powder with 80 mg of KBr and pressing the mixture into a pellet. Over 64 scans were collected for each measurement at a resolution of 4 cm^{-1}.

2.2.4. Field-emission scanning electron microscopy (FE-SEM)

SEM images were recorded on a Hitachi SU8010 cold field emission scanning electron microscope (FESEM, SU8010, Hitachi, Japan) at 1.5 kV accelerating voltage and at a working distance (WD) of 5.0 mm.

2.2.5. Magic angle spinning nuclear magnetic resonance spectroscopy (MAS NMR)

^{27}Al and ^{29}Si MAS NMR spectra were obtained on Bruker AVANCE III 600 spectrometer at resonance frequencies of 156.4 and 119.2 MHz, respectively. ^{29}Si MAS NMR spectra with high-power proton decoupling were recorded on a 4 mm probe with a spinning rate of 12 kHz, a π/4 pulse length of 2.6 μs, and a recycle delay of 80 s. The chemical shifts of ^{29}Si were referenced to tetramethylsilane (TMS). A 4 mm HX double-resonance MAS probe was used to measure ^{27}Al MAS NMR at a sample spinning rate of 14 kHz. The spectra were recorded by a small-flip angle technique with a pulse length of 0.5 μs (<π/12) and a 1 s recycle delay. The chemical shift of ^{27}Al was referenced to 1 M aqueous $Al(NO_3)_3$. The deconvolution of ^{27}Al and ^{29}Si MAS NMR spectra was undertaken using a Gauss–Lorentz cross-product function applied by the PEAKFIT software package. The positions and areas of peaks were obtained until the squared correlation coefficients $r^2 \geq 0.995$.

3. Results and discussion

3.1. Crystallinity and morphology of the synthetic saponites

XRD patterns of the synthetic samples (Fig. 1) displayed the characteristic (001) reflections at ca. 6.5° (2θ) with the d-values of ca. 13.0 Å. All d-values of the (060) reflections were equal to or larger than 1.53 Å, suggesting that trioctahedral saponite was successfully synthesized (Grauby et al., 1993). With a decrease of Mg/Zn ratio, the basal reflection intensity was prominently increased with a decrease of the full width at half maximum, implying an increase of crystallinity and layer stacking order (He et al., 2014). Meanwhile, a small quantity of hemimorphite ($Zn_4Si_2O_7(OH)_2 \cdot H_2O$) formed in the case of Sap-Mg0Zn6, where no Mg^{2+} was added in the preparation solution. The appearance of hemimorphite was probably due to a high pH value and high Zn^{2+} concentration in the reaction system (Yokoyama et al., 2006).

The synthetic Mg-saponites (Sap-Mg6Zn0) exhibited plate-like morphology with curved edges (Fig. 2), which was typically able to be observed in raw clay minerals, especially in smectite family of clay minerals (Cravero et al., 2000; Christidis, 2001). With decreasing in the Mg/Zn ratio, there were more curved edges in Sap-Mg4Zn2 (Fig. 2b) than those in Sap-Mg6Zn0. Well-known rose-like morphology was displayed in Sap-Mg2Zn4 and Sap-Mg0Zn6 (Ma and Pierre, 1999).

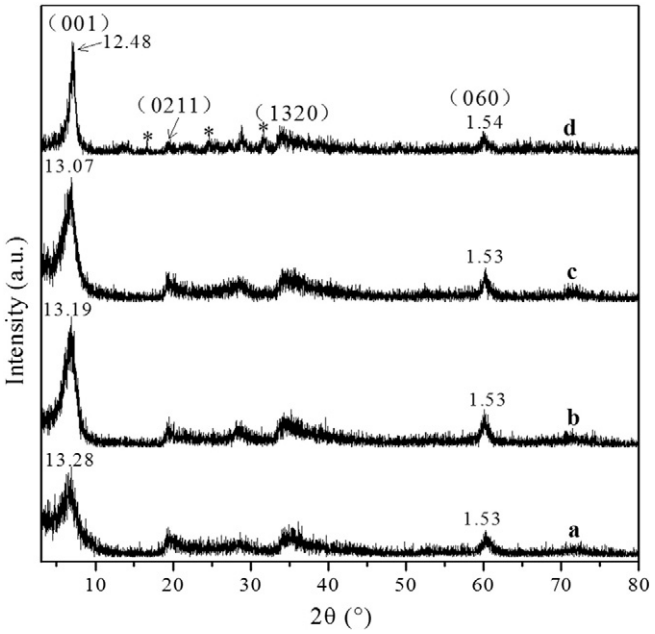

Fig. 1. XRD patterns of synthetic saponite. Sap-Mg6Zn0 (a), Sap-Mg4Zn2 (b), Sap-Mg2Zn4 (c), and Sap-Mg0Zn6 (d). * = Hemimorphite.

3.2. Occupancy selectivity of cations and its influence on microstructure of synthetic saponite

MAS NMR has been demonstrated a powerful technique to determine the local environments for certain atoms (e.g., Al and Si) (Lipsicas et al., 1984). ^{27}Al MAS NMR spectra of the synthetic saponites (Fig. 3) displayed a strong signal of 4-coordinated Al (Al(IV)) at 65–68 ppm and a weak one of 6-coordinated Al (Al(VI)) at ca. 10 ppm, similar to those reported in literature (Vogels et al., 2005a; He et al., 2014). The significant difference between the Al(IV) and Al(VI) signal intensity suggested that Al atoms preferentially occupied tetrahedral sites in *Si*-O tetrahedral sheets via substitution of Al^{3+} for Si^{4+}. With the decrease of Mg/Zn ratio, the intensity of Al(VI) signal decreased significantly, whereas that of Al(IV) increased. Since the Si/Al/(Mg + Zn) ratio was fixed and the ratio of Mg/Zn was varied in the syntheses of saponites, the increase of Al(IV) signal with the decrease of Mg/Zn ratio suggested that the nature of cations in octahedral sites and their relative concentrations had a significant effect on the occupancy of Al atoms in saponite. That is to say, the occupancy of Zn in octahedral sites negatively affected the occupancy of Al in octahedral sites.

Here, ionic radius may be a key factor to control their occupancy, which has a further influence on crystallinity and layer stacking of synthetic saponites. The ionic radii of Al^{3+}, Mg^{2+}, and Zn^{2+} in an octahedron of phyllosilicates are 0.535, 0.72, and 0.74 Å, respectively (Shannon and Prewitt, 1969; Brtndle and KrrKewe, 1979). From the point of ionic radius, a substitution between Mg^{2+} and Zn^{2+} is more readily to happen than that of Al^{3+} for Mg^{2+} or Zn^{2+}. A slight smaller ionic radius of Mg^{2+}, in comparison to that of Zn^{2+}, resulted in more Al^{3+} in Mg-saponite than that in Zn-saponite as evidenced by ^{27}Al MAS NMR spectra.

Our previous study on Mg-saponite with different Si/Al ratios showed that Al(IV)/Al(VI) ratio had an important influence on the crystallinity of synthetic saponite (He et al., 2014), i.e., the larger Al(IV)/Al(VI) ratio, the higher crystallinity. This viewpoint was further confirmed by the present study. The deconvolution of ^{27}Al MAS NMR spectra (Fig. 3) suggested that, with a decrease of Mg/Zn ratio, Al(IV)/Al(VI) ratio dramatically increased from 8.76 for Sap-Mg6Zn0 to 85.55 for Sap-Mg0Zn6. Simultaneously, both the crystallinity and layer stacking order were obviously increased as indicated by XRD patterns (Fig. 1). This is consistent with previous studies that Zn-saponite has higher crystallinity than Mg-saponite (Leliveld et al., 1998; Vogels et al., 1995, 2005b).

^{29}Si MAS NMR spectra provided supporting evidences for Al occupancy in synthetic saponites. ^{29}Si spectra of the synthetic samples (Fig. 4) displayed three signals at approximately −94, −90 and −85 ppm, corresponding to $Q^3Si(0Al)$, $Q^3Si(1Al)$ and Q^2Si [$Q^m(nAl)$, Q^m (m = 0, 1, 2, 3, 4) refers to the polymerization state of Si, and nAl (n ≤ m) to the number of Al in the next-nearest neighbor tetrahedral position], respectively (Lipsicas et al., 1984; He et al., 2014). The Q^2Si unit is located at the layer edges and is of high importance for the surface reactivity of clay minerals (Vogels et al., 2005b; He et al., 2014; Tao et al., 2016).

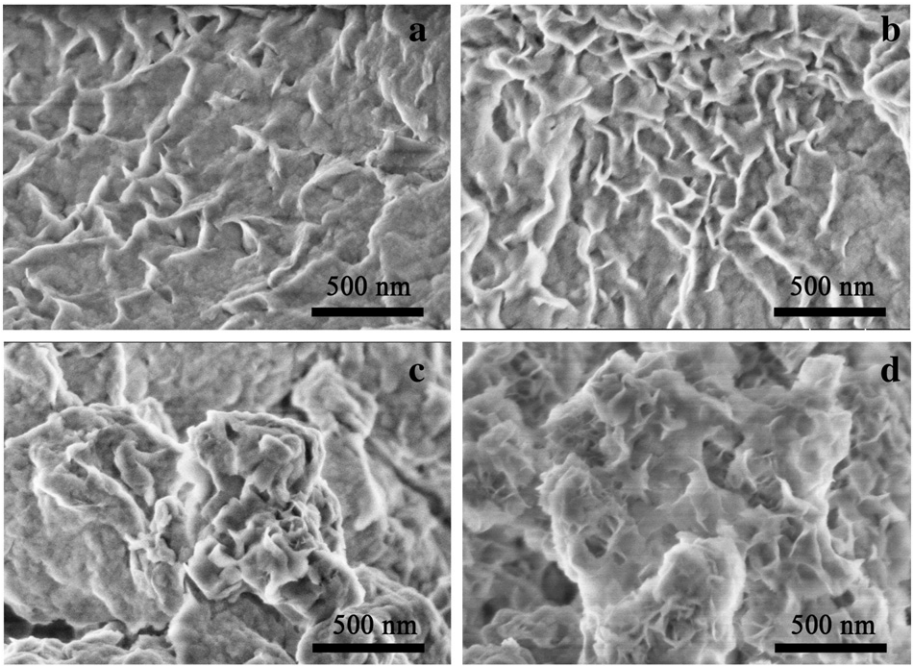

Fig. 2. SEM images of synthetic saponites. Sap-Mg6Zn0 (a), Sap-Mg4Zn2 (b), Sap-Mg2Zn4 (c), and Sap-Mg0Zn6 (d).

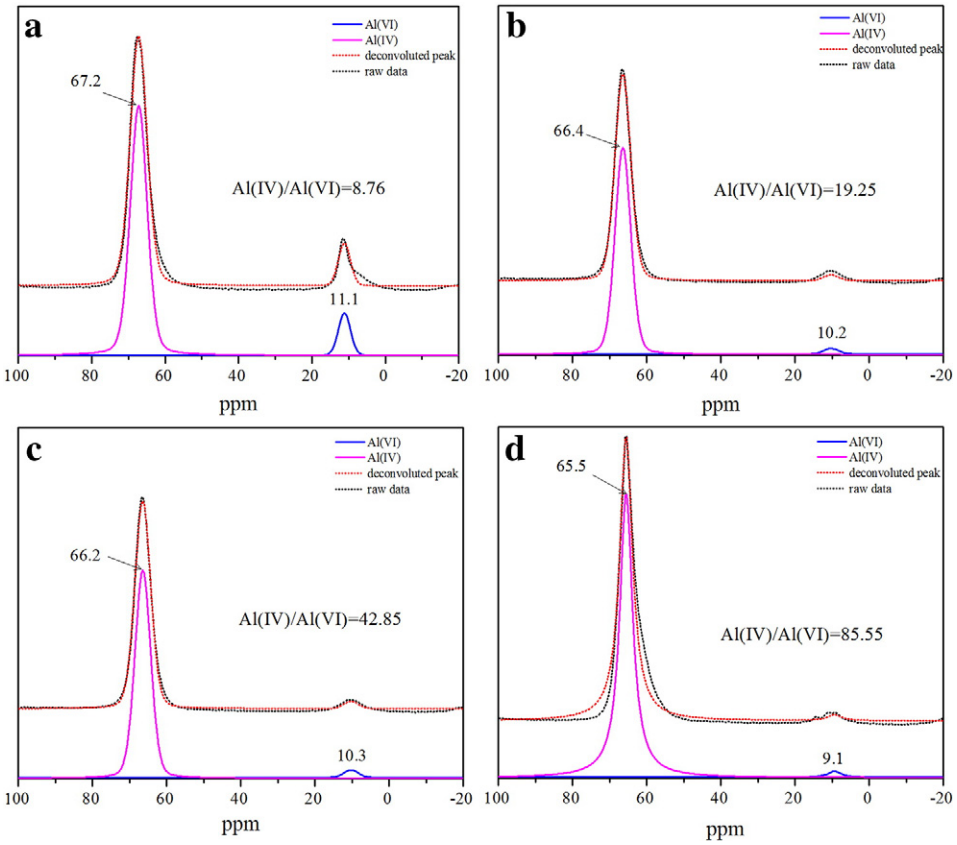

Fig. 3. ^{27}Al MAS NMR spectra of synthetic saponites and their deconvolution results. Sap-Mg6Zn0 (a), Sap-Mg4Zn2 (b), Sap-Mg2Zn4 (c), and Sap-Mg0Zn6 (d).

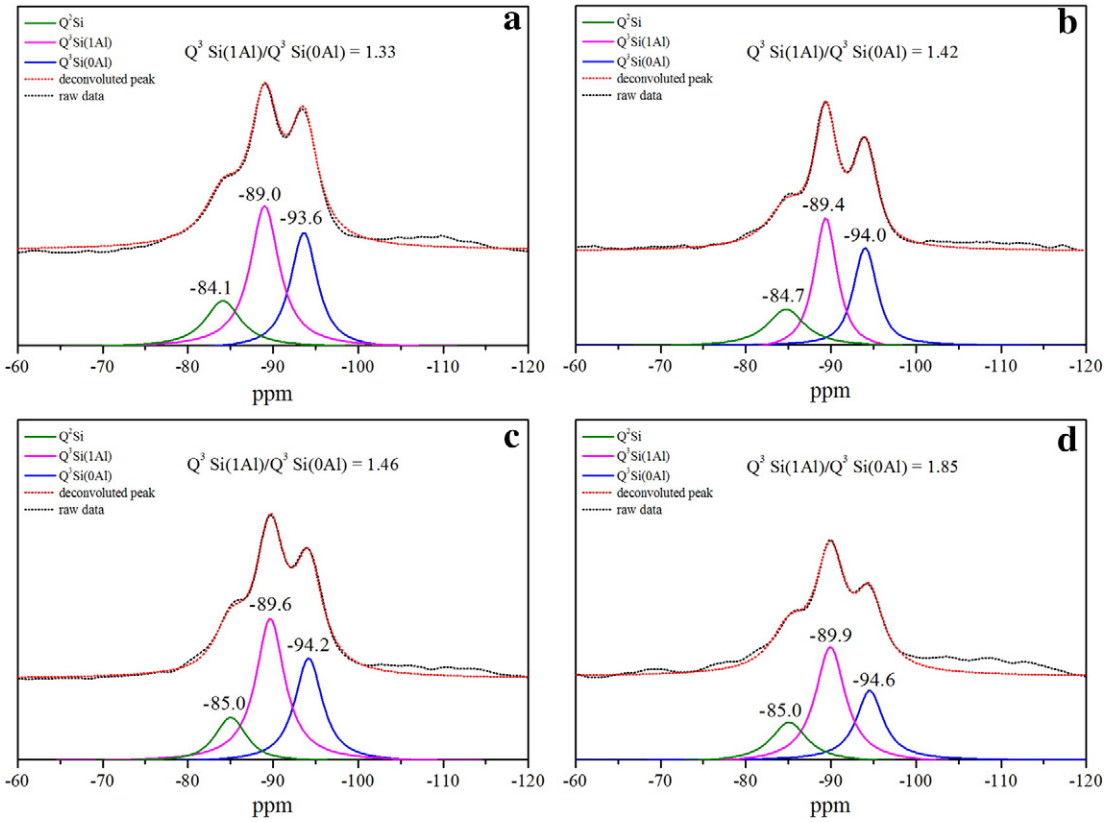

Fig. 4. ^{29}Si MAS NMR spectra of synthetic saponites and their deconvolution results. Sap-Mg6Zn0 (a), Sap-Mg4Zn2 (b), Sap-Mg2Zn4 (c), and Sap-Mg0Zn6 (d).

As revealed by the ^{29}Si MAS NMR spectra, well-crystallized synthetic saponites had a higher $Q^3Si(1Al)/Q^3Si(0Al)$ ratio than the poorly crystallized ones (Fig. 4). The higher $Q^3Si(1Al)/Q^3Si(0Al)$ ratio suggested that more Si^{4+} were substituted by Al^{3+} with the decrease of Mg/Zn ratio. For synthetic saponite with low Mg/Zn ratio, the increased Zn^{2+} in octahedral sites led to an enlargement of the octahedron size in the crystal structure of saponite (Hazen and Wones, 1972). As a result, a bigger tetrahedral sheet, resulted from an increasing substitution of Al^{3+} for Si^{4+}, was required to make size matching between tetrahedral and octahedral sheets.

3.3. Substitution modes of Al^{3+} for Mg^{2+} and Zn^{2+} in octahedral sheet

FTIR spectra provided the evidences for better understanding the occupancy of cations in the synthetic saponites (Fig. 5). The vibrations at 3400–3600 and 1640 cm^{-1} corresponded to stretching and bending vibration modes of OH groups in adsorbed water, respectively (Fig. 5A). The stretching vibration of *Si*-O-Si occurred at around 1000 cm^{-1}, while the bending vibration of *Si*-O-M (M = Mg and Zn) appeared at 430–460 cm^{-1} (Kloprogge and Frost, 2000). With the decrease of Mg/Zn ratio, the frequency of Si-O-M bending vibration shifted from 469 to 447 cm^{-1}. This change was resulted from that the bond energy of Zn-O (332 kJ/mol) was lower than that of Mg-O bond (362 kJ/mol) (Ryan and Huertas, 2013), reflecting that more and more Zn occupied octahedral sites. The prominent band centered at 675 cm^{-1} in Sap-Mg0Zn6 is mainly due to O-*Si*-O bending vibration of hemimorphite (Frost et al., 2007; Li et al., 2013).

Structural —OH vibrations in saponite are mainly affected by the octahedral cations they coordinated. Therefore, the substitution of cation and environment of octahedral sheets may lead to the shift in the position of octahedral —OH vibrations. (Robert et al., 1988; Petit et al., 1995; Besson and Drits, 1997). The bands in the region of 789–818 cm^{-1} (Fig. 5B) were assigned to Si-O-Al deformation modes, corresponding to the 6-coordinated Al in octahedral sheets (Frost and Rintoul, 1996; Kloprogge and Frost, 2000). The increased intensity and blue shift of this vibration with the increase of Zn reflected a prominent increase of the substitution extent of Al^{3+} for M^{2+} (M = Mg and Zn). This conclusion was consistent with the results deduced from ^{27}Al and ^{29}Si MAS NMR spectra, and was also confirmed by the frequency shift of the M-OH (M = Mg, Zn and Al) bending vibration. The vibration at 655 cm^{-1} in Sap-Mg6Zn0 (Fig. 5B), attributed to δMg_3OH (Frost and Rintoul, 1996; Kloprogge and Frost, 2000), shift to a low frequency, approximately 620 cm^{-1}, with the replacement of Zn for Mg in $M_3(OH)$ (M = Mg or Zn). Simultaneously, the other one at 695 cm^{-1}, corresponding to δM_2Al-OH (M = Mg or Zn) (Decarreau et al., 1992; Higashi et al., 2002; Petit et al., 2008), also moved to a low frequency (approximately 620 cm^{-1}) with the decrease of Mg/Zn ratio and Al content in octahedral sheet. For the substitution of Al^{3+} for Mg^{2+} in the octahedral sheet of saponite, two modes have been proposed, i.e., the muscovite substitution (i.e., $3Mg^{2+} = 2Al^{2+}$ + vacancy) and one-to-one substitution (i.e., $1Al^{3+} \rightarrow 1\ Mg^{2+}$) (Suquet et al., 1981; He et al., 2014). As indicated by XRD patterns (Fig. 1), the d-value of (060) reflection larger than 1.53 Å suggested that the synthetic saponites had a tri-octahedral structure. Hence, the lack of the δAl_2OH vibration at around 900 cm^{-1} (Madejova, 2003) and the splitting of the M-OH (M = Mg, Zn and Al) bending vibration in FTIR spectra suggested that the substitution of Al^{3+} for Mg^{2+} or Zn^{2+} in octahedral sheet was one-to-one mode instead of the muscovite substitution mode. Meanwhile, the splitting of bending vibration (Arrow 1 and 2 in Fig. 5B) suggested that Al^{3+} in the octahedral sheets was random (Decarreau et al., 1992).

3.4. Influence of metals in octahedral sheets on the thermal stability of saponite

TG analyses (Fig. 6) showed that the mass loss below 200 °C, corresponding to the desorption of physically adsorbed water and interlayer water associated with interlayer cations, was 10.7% for Sap-Mg6Zn0, 10.1% for Sap-Mg4Zn2, 9.2% for Sap-Mg2Zn4, and 5.7% for Sap-Mg0Zn6, respectively. The mass losses in the temperature range of 500–850 °C were attributed to dehydroxylation of the synthetic saponites. Dehydroxylation of Sap-Mg0Zn6 occurred around 520 °C while that of Sap-Mg2Zn4 happened in a large temperature range, centered at approximately 680 °C. For Sap-Mg4Zn2 and Sap-Mg6Zn0, two well resolved peaks were recorded in DTG curves, which centered at 700 and 835 °C for Sap-Mg4Zn2, and 720 and 835 °C for Sap-Mg6Zn0, respectively. The thermal analyses indicated that the dehydroxylation temperature of synthetic saponites significantly increased with the increase of Mg/Zn ratio and the substitution of Al^{3+} for M^{2+} (M = Mg and Zn). In other words, the nature of metals in octahedral sheet had a significant effect on the thermal stability of saponite. In the case of Sap-Mg0Zn6, Zn^{2+} is the dominant cation in octahedral sites with a minor of Al^{3+} substitution for Zn^{2+}. Hence, the dehydroxylation temperature depended mainly on the strength of Zn-O (332 kJ/mol). With

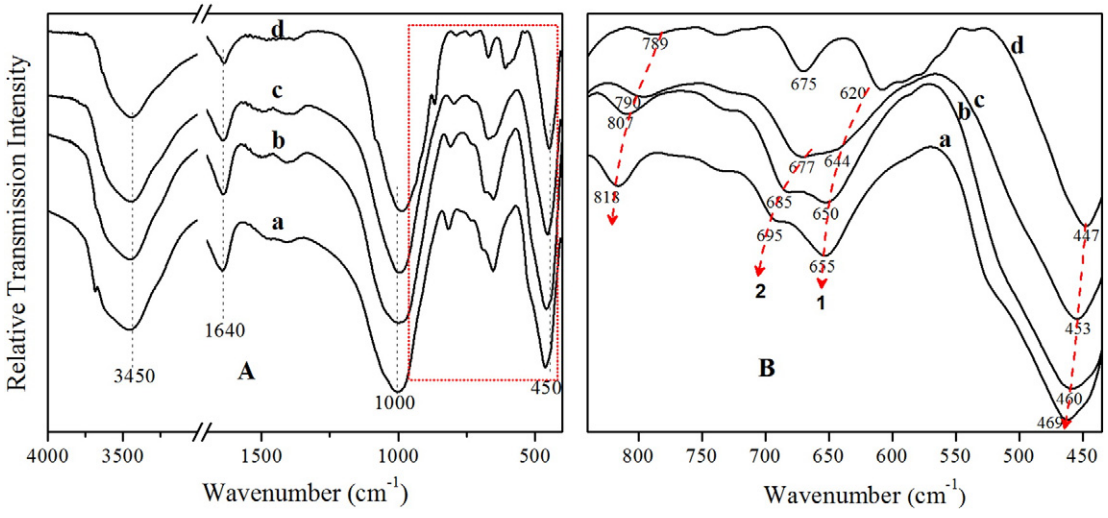

Fig. 5. FTIR spectra of synthetic saponites at 400–4000 cm^{-1} (**A**) and 435 –840 cm^{-1} (**B**). Sap-Mg6Zn0 (a), Sap-Mg4Zn2 (b), Sap-Mg2Zn4 (c), and Sap-Mg0Zn6 (d).

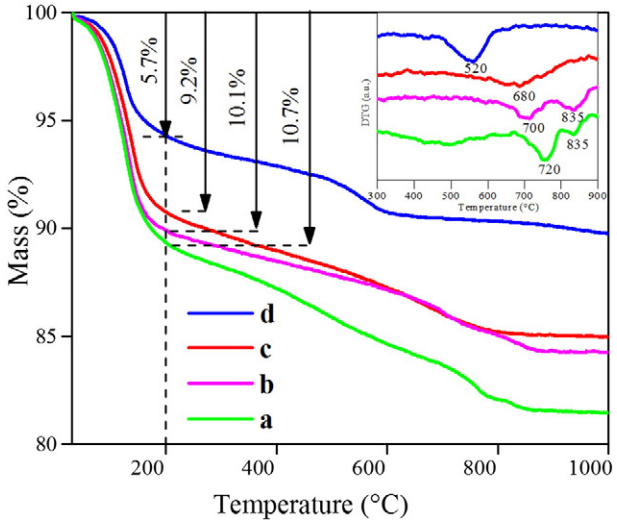

Fig. 6. TG-DTG curves of synthetic saponites. Sap-Mg6Zn0 (a), Sap-Mg4Zn2 (b), Sap-Mg2Zn4 (c), and Sap-Mg0Zn6 (d).

an increase of Mg/Zn ratio, the octahedral sites were simultaneously occupied by both Zn^{2+} and Mg^{2+}. The relatively higher bond energy of Mg-O (362 kJ/mol), compared to that of Zn-O, led to an increase of dehydroxylation temperature. The Al-O bond with higher bond energy (511 kJ/mol) caused higher dehydroxylation temperature for saponite with higher Al content and Mg/Zn ratio such as Sap-Mg6Zn0 and Sap-Mg4Zn2 (Ryan and Huertas, 2013). Accordingly, the dehydroxylation, occurring at the temperature range of 520–720 °C, should be related to Zn and Mg in the octahedral sheets while that at 835 °C to Al in the octahedral sheets. It is noteworthy that the dehydroxylation temperature of Al-OH in synthetic saponite is obviously higher than that in natural montmorillonite, which is 550–700 °C reported in literature (Drits et al., 1995). Montmorillonite has di-octahedral structure, i.e., only two thirds of octahedral sites are occupied by Al while the other one is vacant. However, all octahedral sites in saponite are occupied by metals (e.g., Mg, Zn and Al in this study). The structural difference may result in the dehydroxylation temperature variation of Al-OH in saponite and montmorillonite.

4. Conclusion

In this study, saponites with different Mg/Zn ratio were synthesized under hydrothermal condition. XRD patterns indicated that the reflection intensity obviously increased and its full width at half maximum decreased with a decrease of Mg/Zn ratio, implying an increase of crystallinity and layer stacking order of the synthetic saponites. The rose-like morphology was observed in the SEM images of Zn-saponite. Both ^{27}Al and ^{29}Si MAS NMR spectra suggested that Al atoms preferentially occupy tetrahedral sites. An increase of Zn/Mg ratio in octahedral sites is beneficial for the substitution of Al^{3+} for Si^{4+}, but has negative effect on the substitution of Al^{3+} for Mg^{2+} and Zn^{2+} in octahedral sites. This resulted in an increase of Al(IV)/Al(VI) ratio in synthetic saponites, which is a key factor to control the growth of saponite. FTIR spectra gave further evidence for the substitution of Al^{3+} for Mg^{2+} and Zn^{2+} through one-to-one substitution mode (i.e., $1Al^{3+} \rightarrow 1\ Mg^{2+}/Zn^{2+}$) rather than the muscovite substitution (i.e., $3Mg^{2+} = 2Al^{2+} +$ vacancy). Thermal stability of the synthetic saponites strongly depended on the Mg/Zn ratio in the octahedral sheet as well as the ratio of Al(IV)/Al(VI), i.e., Mg-saponite with low Al(IV)/Al(VI) ratio displayed higher thermal stability than that of Zn-saponite with high Al(IV)/Al(VI) ratio, which mainly corresponded to the bond strength between metal and hydroxyl.

Acknowledgements

This work was financially supported by National Natural Science Foundation of China (Grant Nos. 41530313, 41402038, and 41372048), Guangdong Provincial Youth Top-notch Talent Support Program (2015TQ01Z797), and Team Project of Natural Science Foundation of Guangdong Province, China (Grant No. S2013030014241).

References

Artok, L., Malla, P.B., Komarneni, S., Schobert, H.H., 1993. Intercalated metal clay catalysts in direct liquefaction of bituminous coal. Energy Fuel 7, 430–431.
Besson, G., Drits, V.A., 1997. Refined relationships between chemical composition of dioctahedral fine-grained mica minerals and their infrared spectra within the OH stretching region. 1. Identification of the OH stretching bands. Clay Clay Miner. 45, 158–169.
Bisio, C., Gatti, G., Boccaleri, E., Marchese, L., Superti, G.B., Pastore, H.O., Thommes, M., 2008. Understanding physico-chemical properties of saponite synthetic clays. Microporous Mesoporous Mater. 107, 90–101.
Brat, S., Rajan, N.S.S., 1981. Synthetic magnesium aluminosilicates in radioactive-waste treatment. Indian J Chem A 20, 311–312.
Brtndle, G.W., KrrKewe, S., 1979. A crystal-chemical study of Mg, Al and Ni, N hydroxy-perchlorates and hydroxy-arbonates. Am. Mineral. 64, 836–843.
Casagrande, M., Storaro, L., Lenarda, M., Rossini, S., 2005. Solid acid catalysts from clays: oligomerization of 1-pentene on Al-pillared smectites. Catal. Commun. 6, 568–572.
Chevalier, S., Franck, R., Suquet, H., Lambert, J.F., Barthomeuf, D., 1994. Al-pillared saponites. 1. IR studies. J Chem Soc Faraday T 90, 667–674.
Christidis, G.E., 2001. Formation and growth of smectites in bentonites: a case study from Kimolos Island, Aegean, Greece. Clay Clay Miner. 49, 204–215.
Costenaro, D., Bisio, C., Carniato, F., Gatti, G., Oswald, F., Meyer, T.B., Marchese, L., 2013. Size effect of synthetic saponite-clay in quasi-solid electrolyte for dye-sensititized solar cells. Sol Energ Mat Sol C 117, 9–14.
Cravero, F., Keith, K.S., Murray, H.H., Toth, T., 2000. A white bentonite from San Juan Province, Argentina-geology and potential industrial applications. Appl. Clay Sci. 16, 31–43.
Decarreau, A., Grauby, O., Petit, S., 1992. The actual distribution of octahedral cations in 2:1 clay minerals: results from clay synthesis. Appl. Clay Sci. 7, 147–167.
Drits, V.A., Besson, G., Muller, F., 1995. An improved model for structural transformations of heat-treated aluminous dioctahedral 2:1 layer silicates. Clay Clay Miner. 43, 718–731.
Farmer, V.C., Krishnamurti, G.S.R., Huang, P.M., 1991. Synthetic allophane and layer-silicate formation in SiO_2-Al_2O_3-FeO-Fe_2O_3-MgO-H_2O systems at 23 °C and 89 °C in a calcareous environment. Clay Clay Miner. 39, 561–570.
Frost, R.L., Rintoul, L., 1996. Lattice vibrations of montmorillonite: an FT Raman and X-ray diffraction study. Appl. Clay Sci. 11, 171–183.
Frost, R.L., Bouzaid, J.M., Reddy, B.J., 2007. Vibrational spectroscopy of the sorosilicate mineral hemimorphite $Zn_4(OH)_2Si_2O_7 \cdot H_2O$. Polyhedron 26, 2405–2412.
Grauby, O., Petit, S., Decarreau, A., Baronnet, A., 1993. The beidellite-saponite series: an experimental approach. J Mineral]–>Eur. J. Mineral. 5, 623–635.
Grauby, O., Petit, S., Decarreau, A., Baronnet, A., 1994. The nontronite-saponite series: an experimental approach. J Mineral]–>Eur. J. Mineral. 6, 99–112.
Hazen, R.M., Wones, D.R., 1972. Effect of cation substitutions on physical properties of trioctahedral micas. Am. Mineral. 57, 103.
He, H.P., Li, T., Tao, Q., Chen, T.H., Zhang, D., Zhu, J.X., Yuan, P., Zhu, R.L., 2014. Aluminum ion occupancy in the structure of synthetic saponites: effect on crystallinity. Am. Mineral. 99, 109–116.
Higashi, S., Miki, K., Komarneni, S., 2002. Hydrothermal synthesis of Zn-smectites. Clay Clay Miner. 50, 299–305.
Higashi, S., Miki, H., Komarneni, S., 2007. Mn-smectites: hydrothermal synthesis and characterization. Appl. Clay Sci. 38, 104–112.
Jaber, M., Miehe-Brendle, J., Delmotte, L., Le Dred, R., 2005. Formation of organoclays by a one step synthesis. Solid State Sci. 7, 610–615.
Kawi, S., Yao, Y.Z., 1999. Saponite catalysts with systematically varied Mg/Ni ratio: synthesis, characterization, and catalysis. Microporous Mesoporous Mater. 33, 49–59.
Kloprogge, J.T., Frost, R.L., 2000. The effect of synthesis temperature on the FT-Raman and FT-IR spectra of saponites. Vib. Spectrosc. 23, 119–127.
Kloprogge, J.T., Breukelaar, J., Jansen, J.B.H., Geus, J.W., 1993. Development of ammonium-saponites from gels with variable ammonium concentration and water-content at low-temperatures. Clay Clay Miner. 41, 103–110.
Kloprogge, J.T., Breukelaar, J., Geus, J.W., Jansen, J.B.H., 1994. Characterization of Mg-saponites synthesized from gels containing amounts of Na^+, K^+, Rb^+, Ca^{2+}, Ba^{2+}, or Ce^{4+} equivalent to the CEC of the saponite. Clay Clay Miner. 42, 18–22.
Leliveld, B.R.G., Kerkhoffs, M.J.H.V., Broersma, F.A., van Dillen, J.A.J., Geus, J.W., Koningsberger, D.C., 1998. Acidic properties of synthetic saponites studied by pyridine IR and TPD-TG of n-propylamine. J Chem Soc Faraday T 94, 315–321.
Li, Q.X., Hu, H.P., Zeng, D.W., Chen, Q.Y., 2013. Solubility of hemimorphite in ammonium sulfate solution at 25 °C. T Nonferr Metal Soc 23, 2160–2165.
Lipsicas, M., Raythatha, R.H., Pinnavaia, T.J., Johnson, I.D., Giese, R.F., Costanzo, P.M., Robert, J.L., 1984. Silicon and aluminum site distributions in 2:1 layered silicate clays. Nature 309, 604–607.
Liu, X.H., Breen, C., 2005. High-temperature crystalline phases in nylon 6/clay nanocomposites. Macromol. Rapid Commun. 26, 1081–1086.

Ma, K., Pierre, A.C., 1999. Colloidal behaviour of montmorillonite in the presence of Fe^{3+} ions. Colloid Surf. A 155, 359–372.
Mackenzie, R.C., 1957. Saponite from Allt Ribhein, Fiskavaig Bay, Skye. Mineral. Mag. 31, 672–680.
Madejova, J., 2003. FTIR techniques in clay mineral studies. Vib. Spectrosc. 31, 1–10.
Petit, S., Robert, J.L., Decarreau, A., Besson, G., Grauby, O., Martin, F., 1995. Contribution of spectroscopic methods to 2:1 clay characterization. B Cent Rech Expl 19, 119–147.
Petit, S., Righi, D., Decarreau, A., 2008. Transformation of synthetic Zn-stevensite to Zn-talc induced by the Hofmann-Klemen effect. Clay Clay Miner. 56, 645–654.
Prikhod'ko, R.V., Sychev, M.V., Astrelin, I.M., Erdmann, K., Hensen, E.J.M., Van Santen, R.A., 2003. Nonhydrothermal synthesis and properties of saponite-like materials. Russ. J. Appl. Chem. 76, 700–705.
Reinholdt, M., Miehe-Brendle, J., Delmotte, L., Le Dred, R., Tuilier, M.H., 2005. Synthesis and characterization of montmorillonite-type phyllosilicates in a fluoride medium. Clay Miner. 40, 177–190.
Robert, C., Caulet, J.P., Maillot, H., 1988. Neogene evolution of climate and oceanic circulation in the Ross Sea (Dsdp site-274) deduced from radiolarian microfaunas, clay mineral associations and inorganic chemical-elements. Cr Acad Sci Ii 306, 437–442.
Rodriguez, M.A.V., Barrios, M.S., Gonzalez, J.D.L., Munoz, M.A.B., 1994. Acid activation of a ferrous saponite (griffithite): physico-chemical characterization and surface area of the products obtained. Clay Clay Miner. 42, 724–730.
Ryan, P.C., Huertas, F.J., 2013. Reaction pathways of clay minerals in tropical soils: insights from kaolinite-smectite synthesis experiments. Clay Clay Miner. 61, 303–318.
Shannon, R.D.t., Prewitt, C.T., 1969. Effective ionic radii in oxides and fluorides. Acta Crystall B-Stru B 25, 925–946.
Suquet, H., Malard, C., Copin, E., Pezerat, H., 1981. Variation du paramètre b et de la distance basale d001 dans une série de saponites à charge croissante: I etats hydratés. Clay Miner. 16, 53–67.
Tao, Q., Fang, Y., Li, T., Zhang, D., Chen, M.Y., Ji, S.C., He, H.P., Komarneni, S., Zhang, H.B., Yan Dong, Y., Noh, Y.D., 2016. Silylation of saponite with 3-aminopropyltriethoxysilane. Appl. Clay Sci. 132-133, 133–139.
Trujillano, R., Rico, E., Vicente, M.A., Rives, V., Sobrados, I., Sanz, J., 2015. Saponites containing divalent transition metal cations in octahedral positions - exploration of synthesis possibilities using microwave radiation and NMR characterization. Appl. Clay Sci. 115, 24–29.
Utracki, L.A., 2007. Interphase between nanoparticles and molten polymeric matrix: pressure-volume-temperature measurements. Compos Interface 14, 229–242.
Varma, R.S., 2002. Clay and clay-supported reagents in organic synthesis. Tetrahedron 58, 1235–1255.
Vicente, I., Salagre, P., Cesteros, Y., Medina, F., Sueiras, J.E., 2010. Microwave-assisted synthesis of saponite. Appl. Clay Sci. 48, 26–31.
Vogels, R.J.M.J., Kerkhoffs, M.J.H.V., Geus, J.W., 1995. Non-hydrothermal synthesis, characterisation and catalytic properties of saponite clays. Stud. Surf. Sci. Catal. 91, 1153–1161.
Vogels, R.J.M.J., Breukelaar, J., Kloprogge, J.T., Jansen, J.B.H., Geus, J.W., 1997. Hydrothermal crystallization of ammonium-saponite at 200 °C and autogenous water pressure. Clay Clay Miner. 45, 1–7.
Vogels, R.J.M.J., Kloprogge, J.T., Geus, J.W., 2005a. Synthesis and characterisation of boron and gallium substituted saponite clays below 100 °C at one atmosphere. Microporous Mesoporous Mater. 77, 159–165.
Vogels, R.J.M.J., Kloprogge, V.T., Geus, J.W., 2005b. Synthesis and characterization of saponite clays. Am. Mineral. 90, 931–944.
Yokoyama, S., Tamura, K., Hatta, T., Nemoto, S., Watanabe, Y., Yamada, H., 2006. Synthesis and characterization of Zn-substituted saponite (sauconite). Clay Sci. 13, 75–80.
Zhang, D., Zhou, C.H., Lin, C.X., Tong, D.S., Yu, W.H., 2010. Synthesis of clay minerals. Appl. Clay Sci. 50, 1–11.